Polyethylene Composite Fibers. I. Composite Fibers of High-Density Polyethylene

Waraporn Rattanawijan,[1] Taweechai Amornsakchai[1,2]

[1]*Department of Chemistry and Center of Excellence for Innovation in Chemistry, Faculty of Science, Mahidol University, Phuttamonton 4 Road, Salaya, Nakonpathom 73170, Thailand*
[2]*Center for Alternative Energy, Faculty of Science, Mahidol University, Phuttamonton 4 Road, Salaya, Nakonpathom 73170, Thailand*

Received 23 March 2011; accepted 6 May 2011
DOI 10.1002/app.34863
Published online 5 October 2011 in Wiley Online Library (wileyonlinelibrary.com).

ABSTRACT: Polymer matrix composites are generally studied in the form of bulk solids, and very few works have examined composite fibers. The research described here extended such bulk studies to fibers. The question is whether or not what has been reported for bulk polymers will be the same in fibers. In this article are reported studies of high-density polyethylene (HDPE), whereas those of linear low-density polyethylene are reported in part II of this article series. Two types of filler were used, that is, organically modified montmorillonite (OMMT), in which the nanosized filler particles had a high aspect ratio, and microsized calcium carbonate ($CaCO_3$), with an aspect ratio nearer to unity. Composite fibers of both as-spun and highly drawn forms were prepared, and their structures, morphology, and mechanical properties were studied. It was found that the microsized particles gave HDPE composite fibers with mechanical properties that were the same as those of the neat polymer. In the case of clay composite fibers, the clay interfered with the yield process, and the usual yield point could not be observed. The particle shape did not affect the mechanical properties. The fibers showed different deformation morphologies at low draw ratios. The $CaCO_3$ composite fibers showed cavities, which were indicative of low interaction between the polymer and the filler. The OMMT composite fibers showed platelets aligned along the fibers and good polymer–filler interaction. J Appl Polym Sci 124: 501–509, 2012

Key words: composites; fibers; polyethylene (PE)

INTRODUCTION

Polymer composites are examples of high-performance materials and have a long history, their development having been reported since 1960. These polymer composites are used in many different forms, although not as fibers. In recent years, much progress on reinforcement with fillers with sizes in the nanometer range has been reported. This class is known as *polymer nanocomposites*. As with conventional polymer composites, most previous work has been concerned with bulk polymers. Generally, inorganic nanosized fillers have been incorporated into thermoplastics to improve their mechanical properties over those of the neat polymers. Many works have focused on polymer blends with inorganic fillers, such as calcium carbonate ($CaCO_3$), kaolin, silica, and clay.[1] Most of the published research has indicated that rigid fillers in composite systems, including filled polyethylene (PE), show improved mechanical properties. However, the improvement of the mechanical properties in reinforced materials depend on the filler structure and particularly on the aspect ratio of the reinforcing particles.

Chan, Wu, Li, and Cheung[2] reported that micrometer-sized particles of $CaCO_3$ increased the mechanical properties only slightly because of the relatively low surface area. Their results show a significant increase in the modulus but a negligible increase in yield strength. However, other research revealed a decrease of, or a negligible improvement in, the mechanical properties on the addition filler.[3–8] When the size of the particles is small enough, a dramatic change in the failure mechanism of the polymer from brittle to ductile may occur, as in the case of polyvinyl chloride (PVC).[8] The drawing of polymer composites containing particulate material generally results in the creation of cavities or voids. The effects of the nanoparticle shape on the drawing characteristics were shown by Wang et al.[9]

For reinforcement with platelets having a very high aspect ratio, such as clay, ideally, a significant improvement in the mechanical properties at very

Correspondence to: T. Amornsakchai (sctam@mahidol.ac.th).

Contract grant sponsors: Center for Innovation in Chemistry: Postgraduate Education and Research Program in Chemistry, Commission on Higher Education, Thailand Ministry of Education (to W.R.).
Contract grant sponsor: Thailand Research Fund; contract grant sponsor: RMU5180043 (to T.A.).

low loading would be expected. This point has been clearly illustrated in nylon systems, which are polar materials, and as a result, the clay is fully exfoliated.[10–12] For nonpolar polyolefins such as PE, the level of improvement is much less and varies depending on the degree of dispersion.[13–17] For this nonpolar system, it is difficult to disperse the organomodified clay homogeneously to the same level as can be obtained in the nylon system, so generally a modified polar polyolefin is used as a compatibilizer. This is the polyolefin under study and grafted with maleic anhydride (MA). In some works,[3,18] this modified polyolefin is even used as the matrix.

However, the literature on bulk PE–clay systems is rather inconsistent with regard to the mechanical properties and morphology for both high-density[13–17] and low-density[18–23] systems. There are reports of systems with improved elastic modulus and yield strength values[13–17,20–22] and also with lower tensile properties.[18,19,23] All of this suggested that it was imperative to look at different PE materials and compatibilizer systems to obtain more insight into the relationship between the composite structure and mechanical properties.

However, there have only been a few published works in the field of fibers, so this research work extends such bulk studies to fibers. The research focused on PE fibers because the molecular chains can easily be oriented in the drawing process.

Nowadays, it is accepted that drawing involves five consecutive processes. These were set out (with slightly different numbering) by Brooks et al.,[24] as observed in the stress–strain curve. In process 1, the polymer experiences elastic deformation and recoverable strain. In processes 2 and 3, the nominal stress goes through a maximum, which may involve yield points. In this state, the lamellae start to break and form fibrils; at the same time, the crystal structure can change from orthorhombic to monoclinic. This change is called a *Martensitic transition*. In process 4, the nominal stress is a broad minimum as the neck smoothly elongates and retains a constant thickness until it reaches the extremities of the sample. This phenomenon is called *stable necking*. Finally, in process 5, the stress rises again. This property is known as *strain hardening*. In this region, the extended chains in the remainder of the neck become excessively deformed with a considerable gain of conformation energy and loss of conformational entropy and so oppose further movement. The sample stretches somewhat until, at some weak point, fracture initiates. When filler is added, the composite fibers show altered deformation behavior. So in this work, we examined possible changes in the draw and deformation behavior as a result of the addition of different fillers.

Studies of high-density polyethylene (HDPE) are reported in this article, and those of linear low-density PE are reported in part II[25] of this article series. The fillers were added to the polymer, hopefully to give it improved properties. In this work, two types of filler were used, that is, organically modified montmorillonite (OMMT) and $CaCO_3$. In this study, we also investigated the effect of the shapes (i.e., particulate and platelet) of the fillers. The reason for using OMMT was that the filler particles had a high aspect ratio so that the platelets could be aligned in the oriented polymer, possibly to yield enhanced properties. The reason for using $CaCO_3$ particles was that, in bulk, it lowers the cost and retains the important mechanical properties. So the question was whether or not this would also be the case in fibers. For a clay system, drawing should help orient the clay platelets along the fiber axis, and so this should be an ideal situation to illustrate whether or not clay has reinforcement capability in nonpolar PE.

EXPERIMENTAL

Materials

HDPE, with a melt flow index (ASTM D 1238) of 0.8 g/10 min and grade Thai-Zex 5000S produced by Bangkok Polyethylene, Rayong, Thailand, was used. The material had a density of 0.954 g/cm^3 (ASTM D 1505). Commercial MA-grafted HDPE, known as Fusabond E series grade MB 100D (DuPont, Sarnia, Canada), was used as a compatibilizer. It had about a 1% MA content and a density of 0.96 g/cm^3. The melt flow index was 2 g/10 min. The $CaCO_3$ master batch was supplied by Salee Colour Co., Ltd. (Bangkok, Thailand). The trade name of the $CaCO_3$ master batch was FECC3070. The density of FECC3070 was 1.65 g/cm^3, according ASTM D 1505. The filler master batches were supplied suitably mixed with an HDPE matrix. The mean particle size was 3 μm. The organoclay was commercially available under the trade name Claytone HY, produced by Southern Clay Products. It was purchased from a local distributor and used as received. According to the product literature, the clay was OMMT. Sodium ions in the clay were replaced by alkyl ammonium ions. This was done by a reaction of dimethyl dihydrogenated tallow, having alkyl quaternary ammonium counterions, with the clay. The chemical composition of the hydrogenated tallow units consisted of about 65% C18, about 30% C16, and about 5% C14 chains. The organic cation loading was 125 mequiv/100 g of clay. This particular grade was chosen for this study because it was recommended for low-polarity systems and did not require an activator. The clay was dried in a vacuum oven at 80°C for 24 h before use.

Preparation of the HDPE–$CaCO_3$ (HDCA) composites

The systems of HDPE with microsized $CaCO_3$ were prepared by the mixing of a master batch with neat

TABLE I
Sample Designations and Compositions of Different Composites

Sample designation	Composition			
	HDPE	$CaCO_3$ (wt %)	Clay (phr)	PE-*g*-MA (wt %)
HD	100	0	0	0
HDCA3.47	100	3.47	0	0
HDCA6.94	100	6.94	0	0
HDCA20.82	100	20.82	0	0
HDCL7	100	0	0	7
HDCL7CP3.5	96.5	0	7	3.5
HDCL7CP7	93	0	7	7

polymer in a twin-screw extruder (Prism Engineering, Staffordshire, England) with a temperature profile of 135, 150, 160, 160, and 165°C from hopper to die and a screw speed of 50 rpm. The extruded thread was pelletized. The abbreviation HDCA*Y* represents the high-density polyethylene mixed with $CaCO_3$, where *Y* is the amount of $CaCO_3$. The master batches of $CaCO_3$ had 69.40 wt % $CaCO_3$, as measured by thermogravimetric analysis. The compositions and designations for the various HDPE composite samples are shown in Table I.

Preparation of the HDPE–clay composites

Organoclay can easily be incorporated into molten HDPE, although a considerable time is needed to obtain a homogeneous mix. The composites were prepared by melt-blending with a laboratory two-roll mill at 150–155°C in air at ambient temperature. HDPE was melted on the mill first, and then, a predetermined amount of organoclay was added, and mixing continued until no lumps of organoclay were observed. The mixing time was approximately 20 min. An opaque, pale yellowish composite sheet was obtained. The sheet was then cut into small pellets of about 3×3 mm^2 for subsequent melt spinning. The amount of organoclay in the composites was fixed at 7 wt % HDPE (phr). To study the effect of clay dispersion, compatibilizer was added at 0, 3.5, and 7 wt % of the total polymer. The compositions of the HDPE composite samples are summarized in Table I. The abbreviation HDCL*X*CP*Y* represents the high-density polyethylene mixed with clay and compatibilizer, where *X* is the amount of clay and *Y* is the amount of added compatibilizer.

Melt spinning/hot drawing of the composite fibers

A Randcastle laboratory single-screw extruder (Randcastle Extrusion Systems, Inc., Cedar Grove, NJ) was used to prepare the as-spun fibers. The temperatures of the extruder were set at 120, 180, 190, and 215°C from the hopper to the die zone. The screw speed of 2.2 rpm was used to spin the polymer melt. The instrument unit is shown in Figure 1. HDPE composite pellets were fed at the top, and molten material came out at the bottom through a single-hole spinneret with a diameter of 1 mm. The extrudate was cooled first in air and then by passage through a water bath. The speed of the slow godet was set at around 0.5 m/min and was then slightly adjusted so that the as-spun extrudate had a diameter of around 700 μm. Without breaking the fiber, we drew the as-spun extrudate to many draw ratios in a hot glycerol bath at 113°C. Then, the neat fibers and the composite fibers were drawn in exactly the same way. The draw ratio (DR) was determined by the different winding speeds of the low- and high-speed godet units. The abbreviation DRX represents the X times difference in the speed. The diameters of the resultant drawn fibers were in the range 120–220 μm. The compound with clay was dried in a vacuum oven at 80°C for 24 h before extrusion.

X-ray characterization

Measurements of the state of dispersion and the interlayer spacing of the organoclay in the composites were carried out on a Bruker AXS D8 X-ray diffractometer (Bruker AXS GmBH, Karlsruhe, Germany). A sample size of 30×30 mm^2 was cut from a 1 mm thick compressed sheet and placed in the sample holder of the X-ray diffractometer. The plane of the incident X-ray always made the angle (θ) with

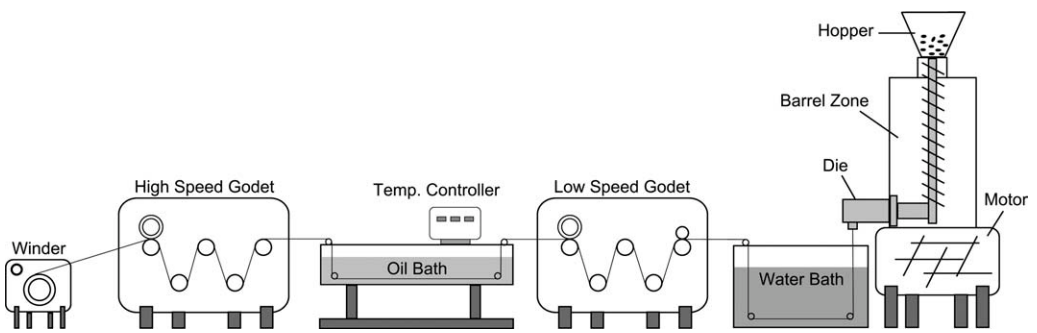

Figure 1 Schematic representation of the fiber-spinning and hot-drawing units.

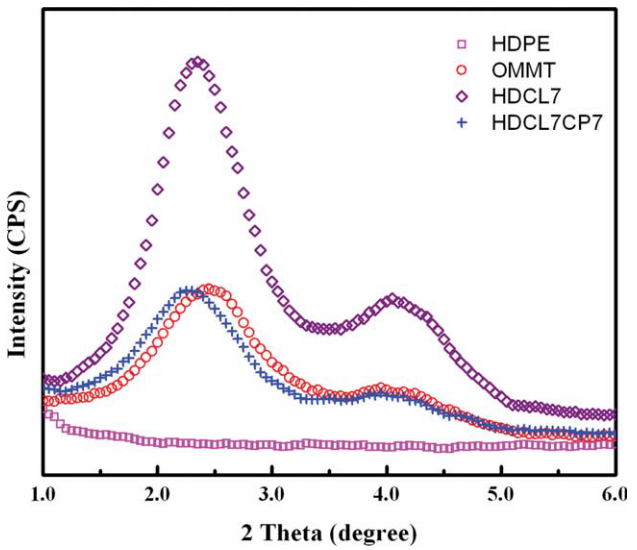

Figure 2 XRD patterns of (□) neat HDPE, (○) pristine clay, (◇) 7-phr clay composite without compatibilizer, and (+) 7-phr clay composite with compatibilizer. [Color figure can be viewed in the online issue, which is available at wileyonlinelibrary.com.]

the sample surface. The scanning angle (2θ) for all of the experiments was between 1 and 6°, and the step size was 0.05°. The X-ray generator was operated at 40 kV and 30 mA.

Tensile testing

The tests were conducted at room temperature with an Instron universal tester (model 5566) (Instron, High Wycombe, England). The tensile specimens were as-spun and drawn fibers, which all had a cylindrical shape. However, the diameter of the specimens depended on the process of drawing [i.e., the as-spun differed from the drawn fibers (see the section on Melt Spinning/Hot Drawing of the Composite Fibers). The distance between the grips was 50 mm in the as-spun fibers and 100 mm in the drawn fibers. The crosshead speed was 50 mm/min for both the as-spun and drawn fibers. Strain was calculated from the grip separation divided by an initial gauge length. The secant moduli at 1% strain and the tensile yield strength were calculated for each specimen. The yield strength was the maximum in the stress–strain curve just beyond the elastic region. An average was taken of seven measurements for each composite composition.

Scanning electron microscopy (SEM)

To observe the internal morphology, the sample surface was cut in the longitudinal direction at a low temperature with a glass knife in a microtome. The exposed surface was etched with a permanganic reagent for 1 h at room temperature. The etchant consisted of a 1% solution of potassium permanganate in mixed acids (10 : 4 : 1 vol % of concentrated sulfuric acid, 85% orthophosphoric acid, and water).[26] The surface morphology of these specimens was observed with a Hitachi model S-2500 scanning electron microscope (Hitachi, Tokyo, Japan) operating at 15 kV.

RESULTS AND DISCUSSION

Structures of the HDPE–clay composites

X-ray diffraction (XRD) is a useful technique for illustrating the dispersion of clay inside the polymer matrix. Because there was no layering in the $CaCO_3$ crystals, no useful measurements could come from XRD, and so the technique was not applied to the $CaCO_3$ systems. The XRD patterns of the 7-phr clay composites with and without compatibilizer are shown in Figure 2. When the clay was added to HDPE, the composites showed a peak slightly that was shifted to a lower angle and with a higher intensity. It is suggested that this was due to intercalation of the polymer into the clay layers without disruption of the ordered structure. The composite with compatibilizer showed low angle scattering but with a significantly lower intensity than composites without compatibilizer. This indicated a degree of disorder in the composites, which, in turn, confirmed better dispersion of the exfoliated clay lamellae in the polymer matrix.[20,23,27–29]

The *d*-spacing data calculated from the (001) peaks are summarized in Table II. The peak of the clay was found at a position of 2.50°, which corresponded to a *d*-spacing of 3.58 nm. In composites without compatibilizer, the peak of the clay was shifted to a slightly lower angle, which corresponded to an increase in *d*-spacing from 3.58 to 3.76 nm. When the compatibilizer was added in a ratio 1 : 1 clay to compatibilizer, the *d*-spacing increased to 3.85 nm. So the conclusion was that the composites without compatibilizer had intercalated structures, whereas the composites with compatibilizer had partially exfoliated structures.

Although there were differences in the structures of the composite fibers, their spinnabilities and drawabilities were almost the same as those of the neat polymer. In this study, it was found that the

TABLE II
Diffraction Peak Angle (2θ) and Corresponding *d*-Spacing (d_{001}) for Neat OMMT and OMMT in the HDCL Composites

Sample	2θ (°)	*d*-spacing (nm)
OMMT	2.50	3.58
HDCL7	2.35	3.76
HDCL7CP7	2.30	3.85

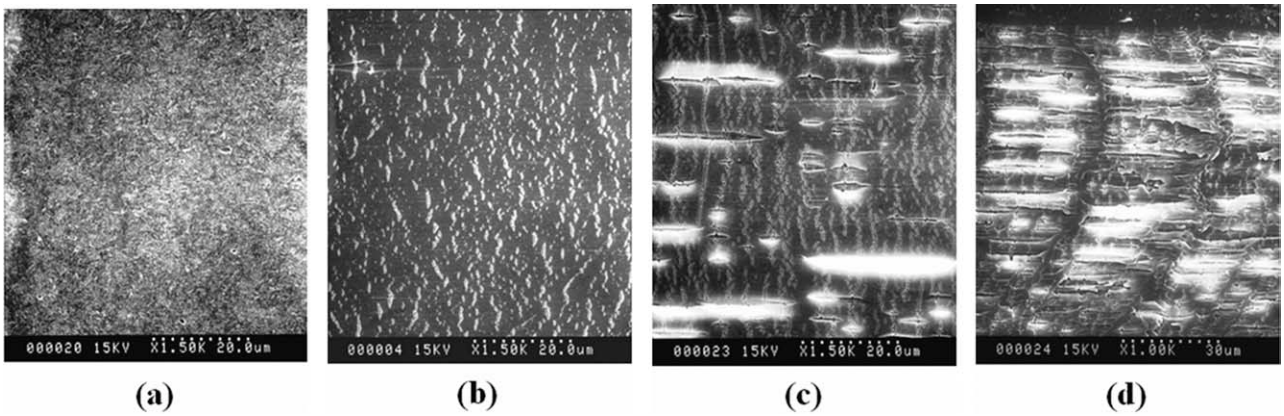

Figure 3 SEM images of HD with a draw direction of left to right: (a) as-spun, (b) DR15, (c) DR20, and (d) DR30.

composites tended to spin to yield slightly smaller diameters when compared with the neat polymer because of the higher composite melt viscosity. So the winding speed was slightly altered to obtain the same diameter for all of the as-spun fibers. This adjustment had no effect on the properties of the as-spun fibers because the spinning was carried out at a relatively low speed (see the section on Melt Spinning/Hot Drawing of the Composite Fibers). All of the composites could be drawn to a draw ratio of 30× the neat polymer, with HDCA3.47 and HDCA6.94 drawn to a slightly higher draw ratio of 35×. The internal morphology and properties of these drawn composite fibers are discussed in the following sections.

Internal morphology of the as-spun and drawn fibers

To understand the tensile properties better, it was helpful to look at the morphology of the composites with SEM. Figure 3(a–d) illustrates the scanning electron micrographs of the etched surfaces of the neat, as-spun HDPE fibers and those with DR15, DR20, and DR30, respectively. The crystalline nature of the as-spun HDPE is shown in Figure 3(a), and it was different from that in the drawn fibers. The drawn fibers showed an intermediate state (called a *metastate*) between the as-spun and the maximum draw ratio. Fibers drawn with DR 15, DR20, and DR30 showed structures with a number of microcracks with long axes perpendicular to the draw direction. The amount of structure increased with increasing draw ratio.

The SEM images of the internal structures of the as-spun and drawn HDCA composite fibers (HDCA6.94 and HDCA20.82) are presented in Figure 4. Both of the as-spun composites fibers showed that the aggregate $CaCO_3$ dispersed randomly in the polymer matrix. The aggregate sizes in HD20.82 were more than 10 μm and were slightly larger than those in HD6.94. In the drawn fibers, again, the polymer matrix showed the intermediate state and microvoid structures. Large voids were clearly seen on the right and the left of the filler particles. The drawn fibers exhibited agglomerated filler particles, and the size of the filler particles was smaller than in the corresponding as-spun materials. This suggested that drawing caused the breakdown of the filler aggregates into smaller sizes.

Figure 5 shows the internal structure of the clay composites fibers without and with compatibilizer. In the composite without compatibilizer, clay particles could be clearly seen. The dispersion of the organoclay was uniform and random. The sizes of the organoclay stacks were bigger than micrometers. With compatibilizer added, the clay particles became much smaller and also largely disappeared. This was consistent with the XRD patterns, which showed a lower scattering intensity in the compatibilized PE composites.

In the drawn organoclay composite fibers, the polymer matrix showed the intermediate state, with a number of microcracks, as seen in the neat fibers. When different fibers with DR20 were compared, the neat fiber showed a small amount of microvoids that were not there with added clay. The number of microcracks in the composites with compatibilizer appeared to be much higher than that in the composite without compatibilizer. No large voids were seen in the high-density polyethylene–clay (HDCL) composite fibers, as in the case of the HDCA composite fibers. The drawn fibers exhibited clay platelets aligned along the draw direction or the fiber axis. It also seemed that the clay particle size became smaller as a result of the drawing process. Simply, by considering the creation and number of microcracks, one could say that the clay changed the nature of the polymer deformation process. This will become more apparent later, when the stress–strain curves of the as-spun composite fibers are considered.

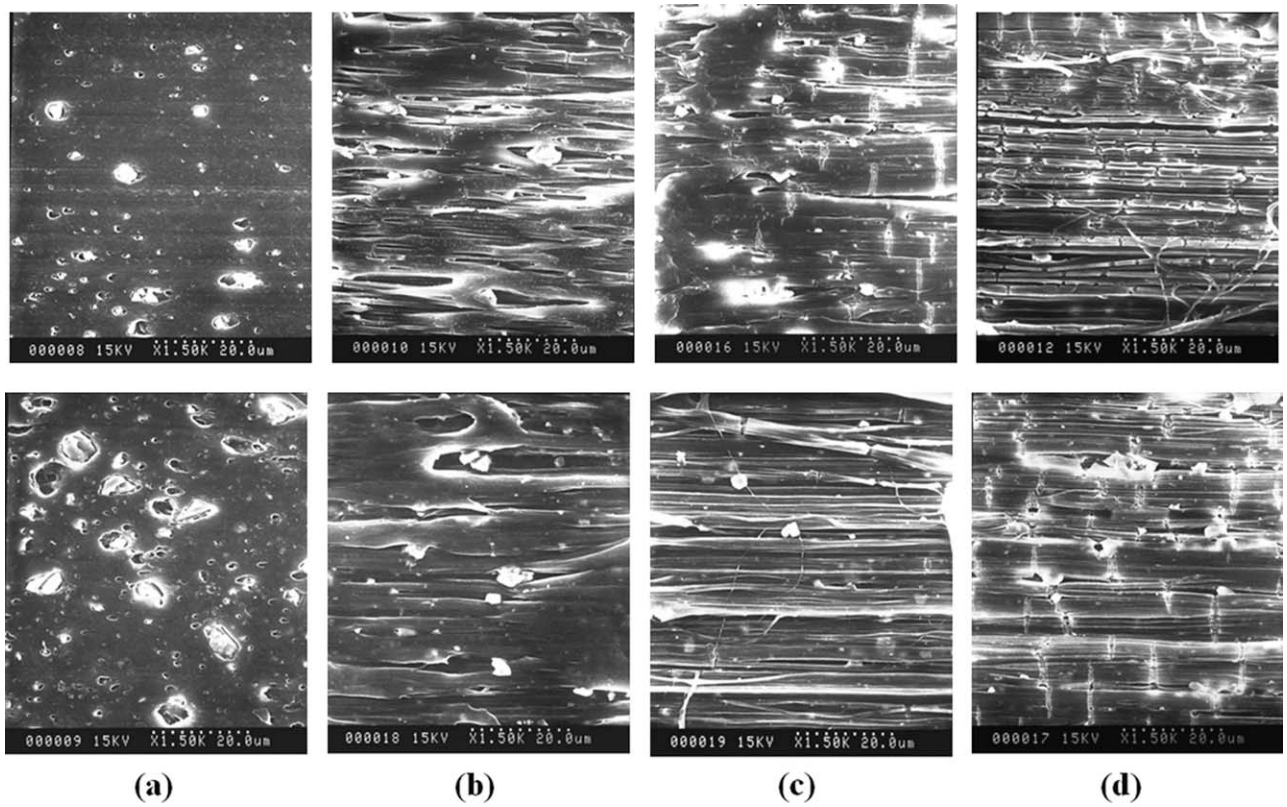

Figure 4 SEM images of HDCA6.94 (top row) and HDCA20.82 (bottom row) with a draw direction of left to right: (a) as-spun, (b) DR10, (c) DR20, and (d) DR30.

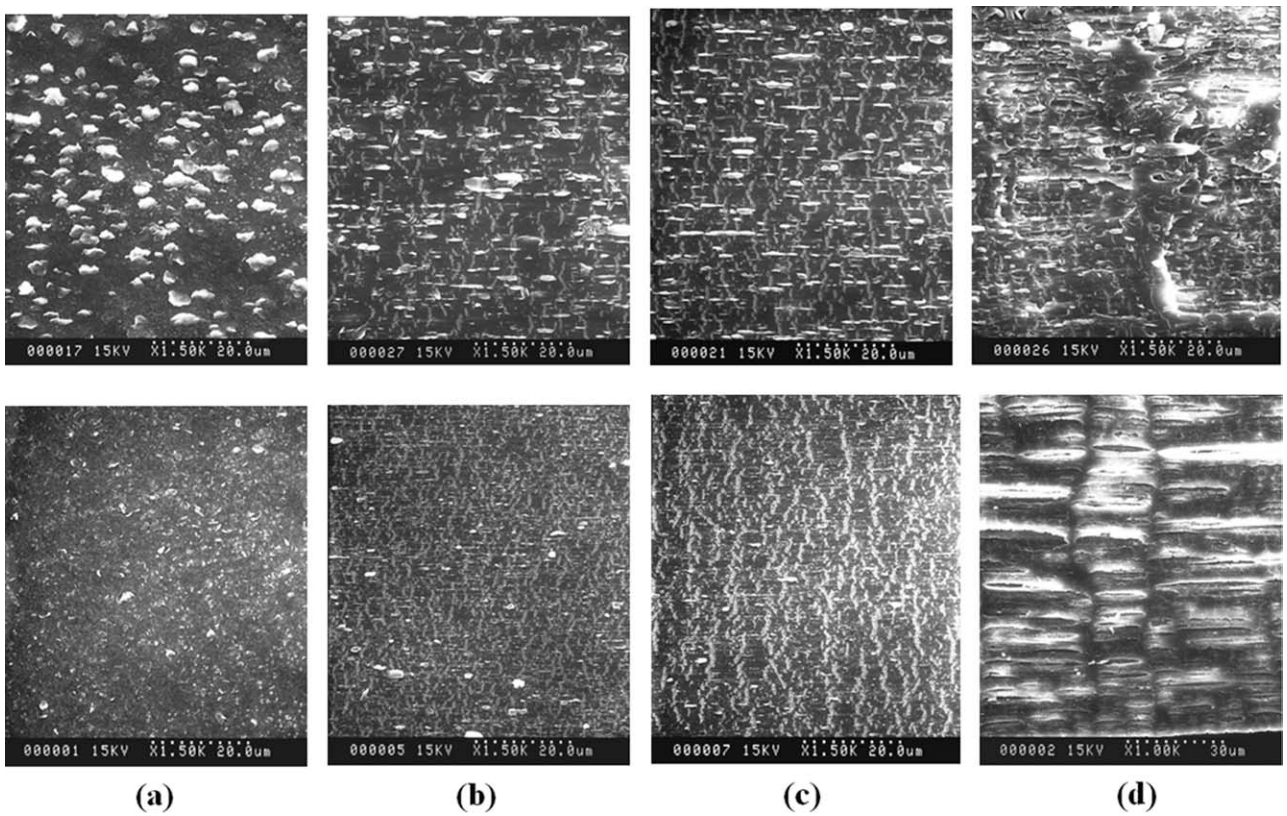

Figure 5 SEM images of HDCL7 (top row) and HDCL7CP7 (bottom row) with a draw direction of left to right: (a) as-spun, (b) DR15, (c) DR20, and (d) DR30.

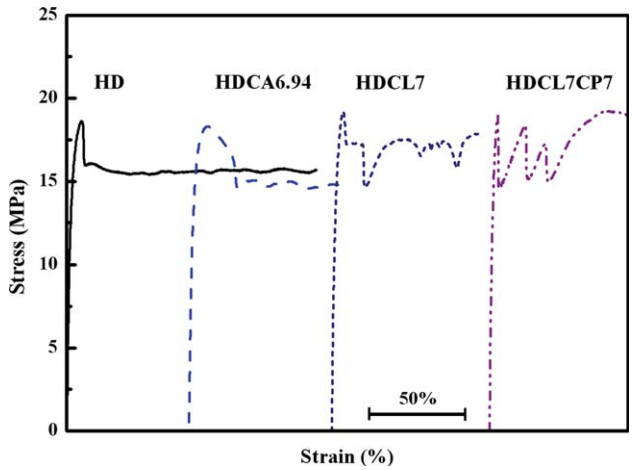

Figure 6 Initial part of the representative stress–strain curves of selected as-spun composite fibers. [Color figure can be viewed in the online issue, which is available at wileyonlinelibrary.com.]

Tensile properties

In this section, we review the stress–strain behavior and tensile properties of the neat and composite fibers. All of the as-spun composite fibers exhibited cold-drawing behavior. To simplify the illustration of too many samples to show on one graph, only those curves with significant information are shown. The representative stress–strain curves of the selected as-spun composite fibers are shown in Figure 6. The neat polymer showed a clear yield point normal for HDPE. With the addition of $CaCO_3$, the composite fiber still showed a clear yield point, but the flow or draw stress became lower than that of the neat polymer. However, when clay was added, the single yield point was replaced by an irregular sawtooth of discontinuous yield points. Apparently, the intercalated clay particles interrupted the smooth flow of polymer molecules in the necking region, and so multiple intermittent necking resulted. The exfoliated clay in the system with compatibilizer made it difficult to identify both the yield point and the drawing stress. In the latter case, if the appropriate part of the curve was considered, the yield stress and flow stress could be regarded as the same.

The significant tensile data for $CaCO_3$ and clay are summarized in Tables III–V. The ultimate tensile strengths are shown in Table III. The ultimate tensile strength increased with increasing draw ratio. At each draw ratio, the strengths of the fibers were practically the same in the neat and composite systems. The maximum draw ratio of composite HDCA20.82 and the clay systems was the same as that of the neat polymer, which were DR10 and DR30, respectively. However, the HDCA3.47 and HDCA6.94 systems could be drawn further than the neat HDPE. In none of these systems was the effect of filler on the ultimate tensile strength greater than the experimental error. So the conclusion was that such fillers had no beneficial effect on the ultimate tensile strength. The natural draw ratio and maximum draw ratio were retained in the composites.

The nominal secant moduli at 1% strain of all of the composite fibers are shown in Table IV. Again, the effects of filler on the nominal modulus were rather small. All of the as-spun and DR10 fibers of the HDCA and HDCL systems appeared to have slightly higher moduli than the neat polymer. For fibers with higher draw ratios, there seemed to be little or no effect of both fillers.

The elongations at break of the composites are presented in Table V. The elongation at break increased with small amounts of solid alone but then decreased with higher amounts of filler. For example, the elongation at break of the as-spun fibers increased from 992 to 1284% but then decreased to 316%. In the drawn fibers, a similar effect was seen at low draw ratios, but the effect was minimal at higher draw ratios.

From the results shown previously, we now attempt to rationalize the effect of $CaCO_3$ and clay on the drawing of the HDPE matrix to fiber. The main difference of the two fillers was that their shapes were spherical particles and platelets, respectively. First, with regard to the addition of $CaCO_3$, this had little or no effect on the cold drawing, modulus, and tensile strength of the composite fibers. $CaCO_3$ particles had a rather low aspect ratio and poor adhesion to the matrix. Drawing tended to

TABLE III
Ultimate Tensile Strengths of the HDCA and the HDCL Composite Fibers (MPa)

	Draw ratio						
Sample	1, as-spun	10	15	20	25	30	35
HD	19 ± 1	300 ± 7	600 ± 30	690 ± 60	720 ± 88	880 ± 89	—
HDCA3.47	24 ± 2	330 ± 50	680 ± 70	810 ± 50	880 ± 38	1000 ± 120	1100 ± 70
HDCA6.94	24 ± 2	370 ± 13	680 ± 45	800 ± 37	792 ± 50	890 ± 40	990 ± 60
HDCA20.82	19 ± 1	320 ± 85	500 ± 24	670 ± 80	870 ± 100	940 ± 60	—
HDCL7	19 ± 1	341 ± 15	590 ± 2	797 ± 27	926 ± 13	956 ± 50	—
HDCL7CP3.5	22 ± 1	—	617 ± 19	728 ± 80	831 ± 32	925 ± 108	—
HDCL7CP7	20 ± 1	327 ± 29	568 ± 19	720 ± 9	780 ± 39	990 ± 50	—

TABLE IV
Nominal Moduli of the HDCA and HDCL Composite Fibers (GPa)

Sample	Draw ratio						
	1, as-spun	10	15	20	25	30	35
HD	0.81 ± 0.02	4.1 ± 0.1	9.6 ± 0.5	16.0 ± 1.7	22.0 ± 3.6	33.0 ± 3.2	—
HDCA3.47	0.98 ± 0.05	4.8 ± 0.9	8.3 ± 2.2	12.8 ± 2.1	22.2 ± 1.2	33.0 ± 3.4	38.5 ± 4.9
HDCA6.94	0.92 ± 0.07	5.2 ± 0.3	10.6 ± 1.2	16.7 ± 1.3	17.4 ± 2.2	25.2 ± 1.4	36.0 ± 5.3
HDCA20.82	0.91 ± 0.02	5.0 ± 1.4	9.3 ± 1.2	14.8 ± 2.8	24.8 ± 6.6	29.5 ± 3.8	—
HDCL7	0.86 ± 0.07	4.9 ± 0.1	8.6 ± 0.5	15.0 ± 1.0	22.0 ± 2.6	26.2 ± 2.1	—
HDCL7CP3.5	0.79 ± 0.11	—	10.0 ± 0.8	15.0 ± 0.7	20.0 ± 0.6	26.0 ± 3.4	—
HDCL7CP7	0.71 ± 0.16	4.9 ± 0.6	10.0 ± 1.1	14.0 ± 1.3	20.0 ± 1.6	30.0 ± 2.8	—

separate the interface that was perpendicular to the drawing direction and, thereby, created large voids and cavities. This is normal for the drawing of polymeric systems containing discrete particles.[9,30] However, these voids did not have any adverse effects on the mechanical properties of the fibers. Presumably, the reinforcing effect of the tightly tied crystallites in the drawn fiber was greater than that of the loosely bound filler particles. It was possible to prepare composite fibers with a high level of $CaCO_3$ loading but with tensile properties similar to the neat fibers. This suggested that with proper choice of $CaCO_3$, a high modulus and high strength fiber could be prepared at a significantly lower cost.

With regard to the HDCL composite fibers, for both the intercalated and exfoliated systems, the clay platelets were partially oriented by either extrusion (in the as-spun polymer) or drawing. Because of the platelet structure, the interface perpendicular to the drawing direction was very small. Hence, no large void or cavities were formed. Similar observations have been reported.[9,31] On the other hand, because of the high aspect ratio and also the alignment of the clay platelets, there was a very high interface area parallel to the drawing direction, which provided sufficient stress transfer to give better reinforcement than the loosely tied spherulitic crystals (below the orientation yield point). In other words, the platelets interfered with the cold-drawing process by stiffening the necked or drawn part, and so a stress drop at a clear yield point was not observed. The addition of compatibilizer caused the platelets to break down into a much greater number and also to become thinner so that the effect became more pronounced, as shown in Figure 6. The increase in resistance to flow or drawout of the material forced the material to accommodate drawing by creating a large number of microcracks, whose major axis was perpendicular to the draw direction. However, the higher reinforcement effect of the exfoliated system appeared to be largely offset by the low-modulus compatibilizer. Because the weight of the compatibilizer on the surface of the clay platelets was less than the total amount, there must have been a lot of the lower modulus compatibilizer in the matrix not bound to the clay. This would have softened the system. The effect of clay was seen only in the as-spun and DR10 fibers. The effect seemed to disappear at high draw ratios. This suggested that the combination of clay and polymer crystallites, now partially converted to oriented lamellae with a different crystal structure and morphology, had roughly the same effect as the now more tightly tied lamellar polymer crystallites alone. This could have been due to two main reasons. The first was the smaller contribution of clay reinforcement compared with the increase in the mechanical properties due to the crystalline and molecular orientation developed over the course of drawing. According to theoretical models, the former should have remained the same (ca. < 1 GPa) throughout the course of drawing, whereas the latter became greater and greater (>10s GPa). The other reason was the weaker interface. Upon drawing to higher and higher draw ratios, because it was only

TABLE V
Elongations at Break of the HDCA and HDCL Composite Fibers as Percentage Strain

Sample	Draw ratio						
	1, as-spun	10	15	20	25	30	35
HD	990 ± 110	21 ± 5	10 ± 1	6 ± 1	4 ± 0.6	4 ± 0.5	—
HDCA3.47	1300 ± 13	70 ± 20	20 ± 3	15 ± 1.6	6 ± 0.3	4 ± 0.5	4 ± 0.3
HDCA6.94	1200 ± 85	30 ± 2	11 ± 0.4	7 ± 0.5	12 ± 2	4 ± 0.3	4 ± 0.7
HDCA20.82	320 ± 330	15 ± 6	7 ± 0.6	6 ± 0.7	4 ± 0.4	4 ± 0.3	—
HDCL7	610 ± 390	30 ± 7	13 ± 1	9 ± 0.5	6 ± 0.7	5 ± 0.7	—
HDCL7CP3.5	600 ± 80	—	12 ± 1	8 ± 1	7 ± 0.5	5 ± 0.3	—
HDCL7CP7	460 ± 200	28 ± 8	12 ± 2	9 ± 0.6	6 ± 0.8	5 ± 0.7	—

the polymer matrix but not the stiff clay platelets that elongated to relieve the imposed drawing stress, the interface became weaker and weaker. In other words, at high draw ratios, the intercrystallite ties became stronger, whereas the crystallite–clay ties became weaker. Despite the general trends described previously, some discrepancies between a certain set of the results was observed, and this indicated that the errors introduced in the whole mixing, extruding, and drawing process could be quite large.

CONCLUSIONS

From these results, we concluded that composite fibers of low-aspect-ratio microsized $CaCO_3$ filler and high-aspect-ratio platelet clay were prepared with properties not too different from the neat fibers. The two fillers did little to alter the extensive polymer crystallite Martensitic transition and reorientation on drawing. So it was no surprise that in the drawn fibers, the tensile properties depended more on the tightly tied oriented polymer crystallite lamellae than on the rather loosely bound filler particles.

The authors gratefully acknowledge the help and advice of A. M. North.

References

1. Wu, D.; Zhou, C.; Zhang, M. J Appl Polym Sci 2006, 102, 3628.
2. Chan, C. M.; Wu, J.; Li, J. X.; Cheung, Y. K. Polymer 2002, 43, 2981.
3. Zhai, H.; Xu, W.; Gua, H.; Zhou, Z.; Shen, S.; Song, Q. Eur Polym J 2004, 40, 2539.
4. Tanniru, M.; Misra, R. D. K. Mater Sci Eng A 2005, 405, 178.
5. Tanniru, M.; Misra, R. D. K.; Berbrand, K.; Murphy, D. Mater Sci Eng A 2005, 404, 208.
6. Deshmane, C.; Yuan, Q.; Misra, R. D. K. Mater Sci Eng A 2007, 452–453, 592.
7. Bartczak, Z.; Argon, A. S.; Cohen, R. E.; Weinberg, M. Polymer 1999, 40, 2347.
8. Wu, D.; Wang, X.; Song, Y.; Jin, R. J Appl Sci 2004, 92, 2714.
9. Wang, K. H.; Chung, I. J.; Jang, M. C.; Keum, J. K.; Song, H. H. Macromolecules 2002, 35, 5529.
10. Fornes, T. D.; Yoon, P. J.; Keskula, H.; Paul, D. R. Polymer 2001, 42, 9929.
11. Fornes, T. D.; Paul, D. R. Polymer 2003, 44, 5013.
12. Powell, C. E.; Beall, G. W. Curr Opin Solid State Mater Sci 2006, 10, 73.
13. Zhao, C.; Feng, M.; Gong, F.; Qin, H.; Yang, M. J Appl Polym Sci 2004, 93, 676.
14. Gopakumar, T. G.; Lee, J. A.; Kontopoulou, M.; Parent, J. S. Polymer 2002, 43, 5483.
15. Zhao, C.; Qin, H.; Gong, F.; Feng, M.; Zhang, S.; Yang, M. Polym Degrad Stab 2005, 87, 183.
16. Osman, M. A.; Rupp, J. E. P.; Suter, U. W. Polymer 2005, 26, 1653.
17. Rattanawijan, W.; Amornsakchai, T.; Amornsakchai, P.; Petiraksakul, P. J Appl Polym Sci 2009, 113, 1887.
18. Su, S.; Jiang, D. D.; Wilkie, C. A. Polym Degrad Stab 2004, 83, 321.
19. Morawiec, J.; Pawlak, A.; Slouf, M.; Galeski, A.; Piorkowska, E.; Krasnikowa, N. Eur Polym J 2005, 41, 1115.
20. Zhong, Y.; Kee, D. D. Polym Eng Sci 2005, 45, 469.
21. Kato, M.; Okamoto, H.; Hasegawa, N.; Tsukigase, A.; Usuki, A. Polym Eng Sci 2003, 43, 6.
22. Hotta, S.; Paul, D. R. Polymer 2004, 45, 7639.
23. Zhang, M.; Sundararaj, U. Macromol Mater Eng 2006, 291, 697.
24. Brooks, N. W.; Duckett, R. A.; Ward, I. M. Polymer 1992, 33, 1872.
25. Rattanawijan, W.; Amornsakchai, T. J Appl Polym Sci submitted.
26. Olley, R. H.; Bassett, D. C. Polym Commun 1982, 23, 1707.
27. Martin, Z.; Jimenez, I.; Angeles Gomez, M.; Ade, H.; Kilcoyne, D. A. Macromolecules 2010, 43, 448.
28. Baghaei, B.; Jafari, S. H.; Khonakdar, H. A.; Rezaeian, I.; As'habi, L.; Ahmadian, S. Polym Bull 2009, 62, 255.
29. Priya, L.; Jog, J. P. J Polym Sci Part B: Polym Phys 2003, 40, 31.
30. Pukanszky, B.; Van es, M.; Maurer, F. H. J.; Vörös, G. J Mater Sci 1994, 29, 2350.
31. Chantrasakul, S.; Amornsakchai, T. Polym Eng Sci 2007, 47, 943.